Theoretical Study of the Molecular and Electronic Structures of Neutral Silver Bromide Clusters $(AgBr)_n$, $n = 1-9$

Hongguang Zhang, Zoltan A. Schelly,* and Dennis S. Marynick*

Department of Chemistry and Biochemistry, University of Texas at Arlington, Arlington, Texas 76019-0065

Received: January 6, 2000; In Final Form: April 17, 2000

The structures and UV absorption spectra of $(AgBr)_n$ clusters ($n = 1-9$) are investigated in both the gas phase and in a dielectric medium. The structures of clusters were determined at the B3P86 level using a moderate size basis set with full geometry optimization. For clusters with $n = 1-6$, extensive searches of the potential energy surface yielded only one minimum, while larger clusters displayed two or more minima. Qualitative aspects of the major UV absorption band were also explored. Experimentally, as the clusters grow from monomers to larger systems, this band initially shifts to the blue and then to the red. Our computational results parallel the experimental trends and show that the maximum blue shift occurs at the trimer or the tetramer. The molecular origin of the blue/red shift associated with AgBr cluster growth can be readily explained by examining the orbital interactions which dominate the process and by the structure characteristics of the clusters. Detailed molecular orbital energy level correlation diagrams for the dimerization, trimerization, and tetramerization are also presented.

Introduction

Extensive studies over the past few decades of nanoscale semiconductor clusters have been fueled by technological and scientific interests, mainly because they exhibit quantum size effects (QSE).[1−3] The main aim of investigations has been toward understanding the changes in structural and electronic properties with varying cluster size.[4] In the nanometer size range, the energy gap of semiconductor clusters was found to decrease with increasing size of the particles, reflected in a red shift of their major UV absorption band.

Because of their application in the photographic process and because of their unique electronic properties, AgBr clusters have received considerable attention[6−8] and the QSE of the particles has been studied by several groups.[9−13] Chen et al., by using a modified reverse micellar synthetic approach, grew clusters of AgBr over a size range of 30−100 Å.[14] From the low-temperature steady state luminescence spectra, they found that the energy gap decreases with increasing cluster size, in good agreement with the Brus formula.[15] He et al. studied the size-dependent UV absorption spectra of AgBr quantum dots and found the major absorption band to undergo a red shift as the cluster size increases.[16] This is the normal QSE and is well understood.[17,18] In contrast, we found that when AgBr clusters are in the molecular size regime, the major absorption band first exhibits a blue shift upon cluster growth. The UV absorption band of silver bromide dimer $(AgBr)_2$ is blue-shifted relative to that of the monomer and only after further cluster growth in the quantum dot size range is the typical red shift observed.[19] More recently, we found that the UV absorption band of AgBr clusters synthesized via the electroporation of unilamellar vesicles first exhibits blue and then red-shifts as the clusters slowly grow in the 5−20 Å range. The ultimate clusters thus formed (∼20 Å) absorb at about 273 nm.[20] The current state of knowledge of the UV absorption spectra associated with the growth of silver bromide clusters is summarized in Figure 1. Clearly, the growth of AgBr clusters in the molecular regime

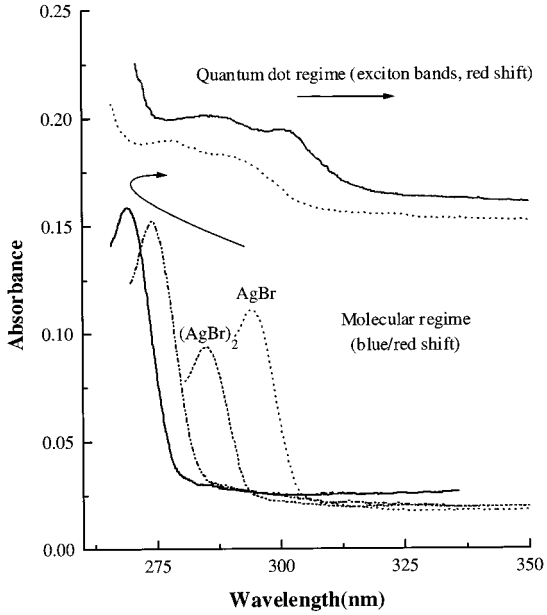

Figure 1. Summary of the current state of UV absorption spectra associated with the growth of silver bromide clusters. For the molecular regime, see refs 19 and 20, for the quantum dot regime, see refs 16 and 19. The arrows indicate the direction of migration of the absorption band.

is associated first with a spectral blue shift followed by a red shift. The turnaround point is at 269 nm. Upon further growth of the clusters in the quantum dot regime, the associated red shift of the split exciton bands is well understood. In this work, we are interested in answering the following questions: What are the molecular structures of the small AgBr clusters that result in the blue/red shifts in the molecular regime and what is the molecular origin of the blue/red shifts?

Considerable theoretical work has been done on systems related to silver bromide clusters, although we are unaware of any report on $(AgBr)_n$, $n > 2$. Both ab initio HF and density

10.1021/jp000099w CCC: $19.00
Published on Web 06/10/2000

TABLE 1: Bond Length (Å) of the AgBr Monomer As Obtained by Various Methods

	bond length	error
experimental	2.3931	
HF/3G	2.1915	−0.2016
HF/SB	2.5052	0.1120
HF/Ldz	2.5676	0.1745
B3P86/SB	2.4250	0.0319
B3P86/LB	2.4618	0.0687
B3P86/LB1[a]	2.4208	0.0227
B3P86/LB2[b]	2.4228	0.0247
B3LYP/SB	2.4416	0.0484
B3PW91/SB	2.4335	0.0404
BP86/SB	2.4230	0.0299
BLYP/SB	2.4417	0.0486
BLYP/LB	2.5002	0.1071
BLYP/LB1	2.4478	0.0517
BLYP/LB2	2.4598	0.0667
BPW91/SB	2.4302	0.0371

[a] LB1: Landz2 basis on Ag,[60] with all orbitals decontracted and an additional 3d function with an exponent of 0.08, 6-31G* plus diffuse functions (exponent = 0.0376) on Br. [b] LB2: Landz2 basis completely uncontracted on Ag + f function (exponent = 0.55),[60] Alrich VTZ plus polarization on Br.[38]

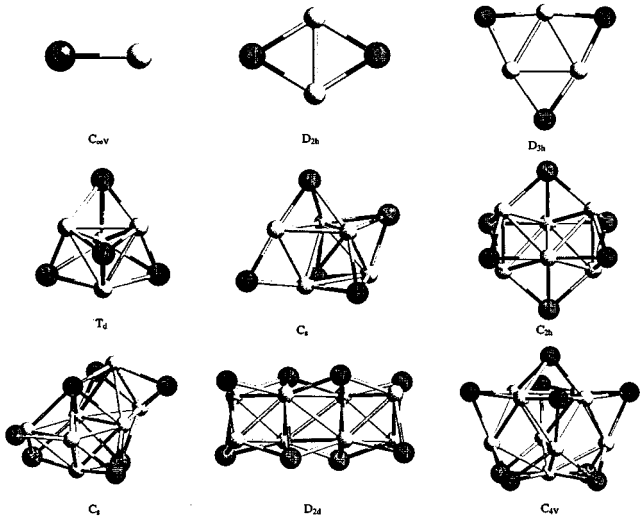

Figure 2. Structures with the lowest energies from the monomer to the nonamer obtained at the B3P86/SB level. The small light spheres represent silver atoms and the large dark spheres represent bromine atoms.

functional theory (DFT) have been used to calculate the band structure of silver bromide crystals.[21−24] The SCF-Xα-SW MO method has been utilized to examine the electronic structure of Ag_2.[25] Ground state and excited state calculations on Ag_3 have been carried out by Walch et al.[26,27] The ground state energies of Ag_6 for four possible structural models were computed using the complete active space multiconfiguration self-consistent field method followed by additional configuration interaction.[28] The ground state geometries of small neutral Ag_n ($n = 2-9$) and cationic Ag_n^+ ($n = 2-9$) clusters have been determined in the framework of the Hartree−Fock and CAS SCF procedures employing relativistic effective core potentials.[29] A systematic quantum-mechanical investigation, with non-local density functionals and a Gaussian basis set, of the stable geometries and energetic characteristics of neutral silver clusters up to the hexamer has appeared.[30] Also, the electronic structures and optical spectra of nanometer-size silver clusters Ag_n ($n = 2-15$) have been determined in the framework of self-consistent-field local density theory. The results show that there is a quantum size effect in Ag_n clusters which can be observed as a red shift

TABLE 2: Geometries (Å, deg) of AgBr Clusters from the Monomer to the Tetramer in the Gas Phase and in a Dielectric Medium ($\epsilon = 78.5$)

clusters (symmetry)	geometries	B3P86/SB gas phase	B3P86/SB dielectric medium
AgBr ($C_{\infty v}$)	R(Ag−Br)	2.4250	2.4865
$(AgBr)_2$ (D_{2h})	R(Ag−Ag)	2.7200	2.7487
	R(Ag−Br)	2.6093	2.6396
	θ(Br−Ag−Br)	117.1717	117.2463
$(AgBr)_3$ (D_{3h})	R(Ag−Ag)	2.8638	2.8919
	R(Ag−Br)	2.5418	2.5652
	θ(Br−Ag−Br)	171.4249	171.378
	θ(Ag−Ag−Br)	55.7125	55.6890
$(AgBr)_4$ (T_d)	R(Ag−Ag)	2.7224	2.7351
	R(Ag−Br)	2.8930	2.9045
	θ(Ag−Br−Ag)	64.1904	64.1437
	θ(Br−Ag−Br)	110.5462	110.5739
	θ(Br−Ag−Ag)	106.8908	106.9198

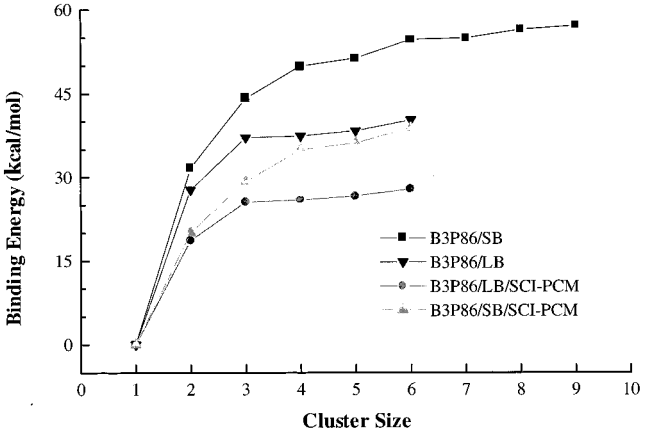

Figure 3. Binding energy as a function of cluster size (n), obtained by different methods.

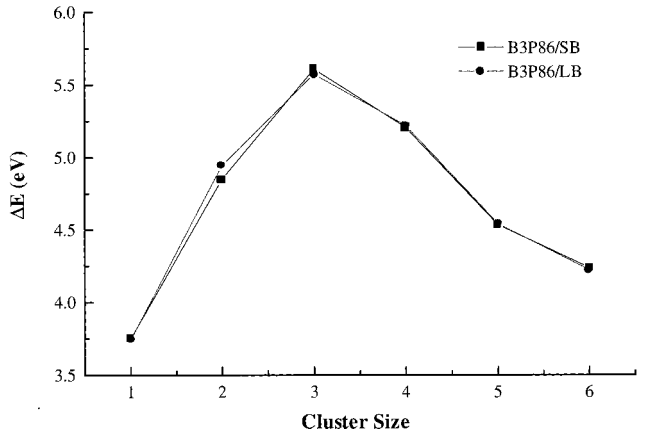

Figure 4. HOMO−LUMO gap as a function of AgBr cluster size (n) from the monomer to the hexamer.

in the absorption threshold and a semiconductor−conductor transition with increasing n.[31,32] The Br_2 molecule has been studied at the Hartree−Fock level.[33] The electronic structure, binding energy, and charge distribution of Br_4^{2-} have been studied using a free electron model for the valence electrons.[34] Ab initio calculations with both all-electron basis sets and effective core potentials (ECP) at the HF and MP2 levels were employed to study the bonding in chainlike Br_5 cations and anions. An electron density analysis based on Bader's theory of atoms in molecules showed that these polyhalogen cations and anions can be described in terms of the VSEPR model. The structural and electronic properties of homoatomic chains consisting of up to five Br atoms were studied by means of the

TABLE 3: Total Energies (au) of $(AgBr)_n$ ($n = 1-9$) Clusters in the Gas Phase and in a Dielectric Medium ($\epsilon = 78.5$)

	gas phase		dielectric medium	
clusters	B3P86/SB	B3P86/LB[a]	B3P86/SB	B3P86/LB[a]
AgBr	−7 740.012 191 93	−7 775.640 037 80	−7 740.039 254 95	−7 775.661 108 43
$(AgBr)_2$	−15 480.125 141 60	−15 551.368 451 70	−15 480.142 433 20	−15 551.381 656 20
$(AgBr)_3$	−23 220.247 696 00	−23 327.097 461 80	−23 220.257 325 20	−23 327.105 355 50
$(AgBr)_4$	−30 960.366 757 20	−31 102.798 429 60	−30 960.380 079 00	−31 102.809 476 20
$(AgBr)_5$	−38700.46976810	−38878.50541930	−38700.48425590	−38878.51755950
$(AgBr)_6$	−46 440.595 397 70	−46 654.224 971 80	−46 440.606 516 70	−46 654.232 998 30
$(AgBr)_7$	−54 180.697 494 80			
$(AgBr)_8$	−61 920.816 452 50			
$(AgBr)_9$	−69 660.928 777 30			

[a] Geometry from calculations at the B3986/SB level.

TABLE 4: Excitation Energies (eV) of AgBr Clusters Modeled by Various Methods

		gas phase HOMO−LUMO ΔE_{HL}		gas phase vertical $\Delta E_{singlet-triplet}$		dielectric medium ΔE_{HL}	dielectric medium $\Delta E_{singlet-triplet}$	CIS method	
clusters	exptl value	B3P86/SB	B3P86/LB	B3P86/SB	B3P86/LB	B3P86/SB	B3P86/SB	B3P86/SB	B3P86/LB
AgBr	4.20	3.75	3.74	3.25	3.27	5.64	4.10	4.44	4.67
$(AgBr)_2$	4.35	4.85	4.94	3.74	3.83	5.55	3.97	5.70	5.96
$(AgBr)_3$	*a*	5.61	5.57	5.44	5.46	5.65	4.40	6.48	6.54
$(AgBr)_4$		5.21	5.22	4.21	4.52	5.42	4.35	6.66	6.78
$(AgBr)_5$		4.53	4.54	3.69	3.69	4.60	3.70	6.10	6.15
$(AgBr)_6$		4.24	4.22	3.28	3.26	4.26	3.57	5.84	
$(AgBr)_7$		4.46							
$(AgBr)_8$		4.49							
$(AgBr)_9$		3.09							

[a] The experimental point of maximum blue shift = 4.61 eV, but the cluster size is not known (ref 206).

DFT approach with a Gaussian basis set and including nonlocal corrections to the exchange and correlation energy.[35] To our knowledge, only one theoretical study is available on free $(AgBr)_n$ clusters. Most recently, Rabilloud et al. reported ab initio configuration interaction (CI) calculations on the ground state of small neutral and singly charged silver bromide clusters $Ag_nBr_p^{(\pm)}$ ($n \leq 2$, $p \leq 2$).[36]

In this paper, we present the results of our computational studies on neutral silver bromide clusters ($(AgBr)_n$, $n = 1-9$) and their UV absorption spectra. HOMO−LUMO energy gaps, singlet−triplet energies, and CIS calculations demonstrate first a blue and then a red shift of the absorption band upon cluster growth which parallel the experimental trends. The molecular origin of the blue/red shift will be explained by use of molecular orbital energy level correlation diagrams.

Computational Details

All calculations were done with the Gaussian 94 suite of the programs.[37] Initially we searched for minima on the potential surface at the HF/STO-3G level. Starting geometries included the following: (1) the AgBr crystal lattice filled with a particular number of AgBr monomers in all possible connected manners; (2) a wide variety of polyhedral structures. For the monomer to the hexamer, only one global minimum was found. For clusters larger than the hexamer, more than one minima were located for each cluster. These structures were subsequently reoptimized at the B3P86/SB level, where SB is a relatively small basis set consisting of 3-21G on Ag and 3-21G* on Br. This approach was tested against a large number of other functionals/basis sets and found to be a good compromise between accuracy and computational time for calculation of the AgBr monomer bond length (see below). For the smaller clusters ($n = 2-6$) we also performed extensive searches of the potential energy surface directly with the SB basis set at the B3P86 level. Analytic frequency calculations were performed in all cases, and structures which did not correspond to a true minimum were distorted along the imaginary frequency until a true minimum was found. Energetics were then reevaluated at the B3P86/LB level. The large basis was constructed as follows: Ahlrichs VTZ+d on Br,[38] and DGauss DZVP on Ag.[39] The silver basis set was enhanced by decontracting the valence d functions from 3/1 to 2/1/1 and adding a set of f functions with an exponent of 0.55. Solvation effects were estimated by reoptimizing the clusters in a dielectric continuum ($\epsilon = 78.5$) at the B3P86/SB and B3P86/LB levels using the self-consistent isodensity polarizable continuum model (SCI-PCM).[40,41] Studies using the large basis set and/or solvation models were restricted to clusters up to the hexamer. Coordinates for all optimized geometries are given in the Supporting Information.

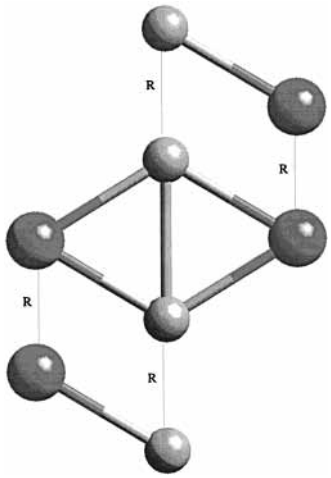

Figure 5. Formation of the dimer from two monomers with overall C_{2h} symmetry.

Results and Discussion

Structures of the AgBr Clusters. Table 1 shows the calculated bond lengths (Å) of the AgBr monomer as obtained by various methods. The experimental value of the bond length is 2.393 Å.[42,43] The calculated values using B3P86,[44,45]

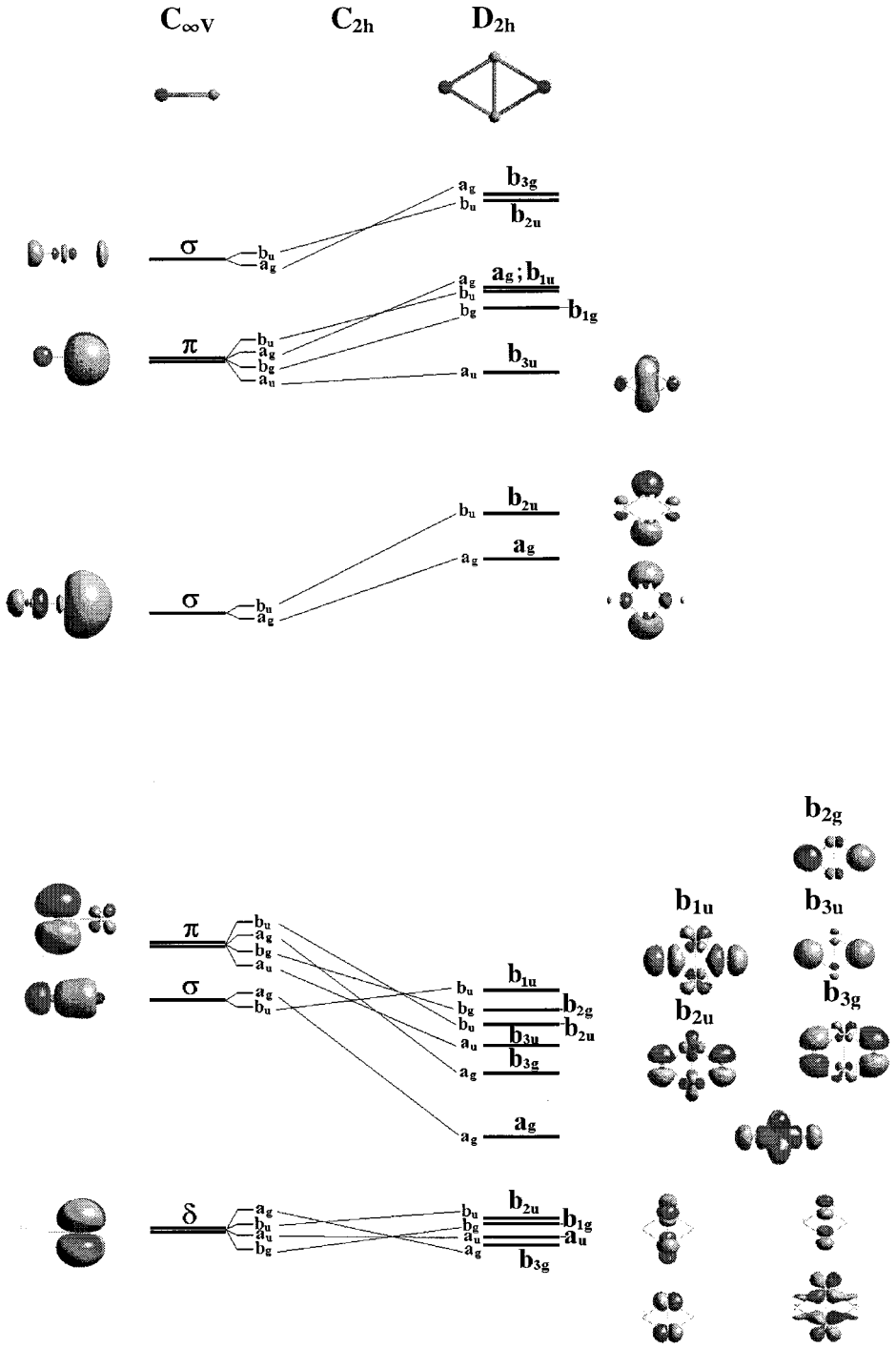

Figure 6. Molecular orbital energy level correlation diagram for dimerization.

B3LYP,[44,46] BP86,[45,47] and BLYP[46,47] functionals with the SB basis set are 2.425, 2.4416, 2.423, and 2.4417 Å, respectively. All of them are reasonably close to the experimental value: The smallest error is 0.030 Å, and the largest error is 0.049 Å. They are also close to the calculated value of 2.424 Å obtained by MRPT2 method with a much larger basis set.[36] We used the B3P86/SB method to reoptimize the structures. Figure 2 shows all the minima with the lowest energies from the monomer to the nonamer obtained at the B3P86/SB level.

Examination of the dimer, which has D_{2h} symmetry, reveals a relatively short Ag−Ag distance (2.72 Å). This is a persistent feature of all of the AgBr clusters: Clusters of silver atoms are formed with the bromine atoms either capping a face or bridging an edge of the silver polyhedron. The MRPT2 method with a much larger basis set also yielded D_{2h} symmetry for the dimer.[36] The trimer (D_{3h} symmetry) consists of a triangular arrangement of silver atoms with bromines bridging the Ag−Ag bonds. In the tetramer (T_d symmetry), Ag−Ag atoms are arranged in a tetrahedral fashion, with one bromine atom capping each face of the Ag_4 tetrahedron. The tetrahedral arrangement of silver atoms is a common feature of all of the larger clusters up to and including the hexamer. The pentamer is best described as two Ag_4 tetrahedra sharing a common face, with the bromine atoms either capping a face of a tetrahedron or bridging an Ag−Ag edge bond to form a structure of C_s symmetry. In the hexamer, the Ag−Ag interactions still result in two Ag_4 tetrahedral structures; however, these two silver tetrahedra now share one common Ag−Ag edge bond. The six bromine atoms

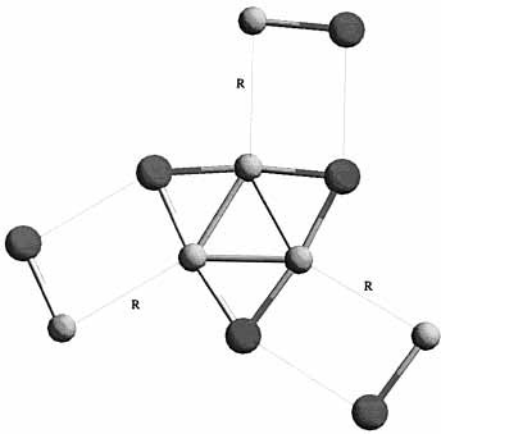

Figure 7. Formation of the trimer from three monomers with overall C_{3h} symmetry.

cap six silver faces to form a structure of C_{2h} symmetry. The hepatamer (C_s symmetry) is the first cluster which cannot be described as a combination of Ag_4 tetrahedra. In this species, there is one Ag_4 tetrahedron sharing a common edge with one Ag_5 square pyramid. The octamer (D_{2d} symmetry) again consists of three tetrahedral Ag_4 units, with the central unit sharing common edges with both remaining tetrahedra. The last cluster, $(AgBr)_9$, is a very open structure quite unlike the others and with a HOMO−LUMO gap that is much lower than that of the first eight clusters. It is likely that other minima exist on the $(AgBr)_9$ surface with lower energies, but the size of this system precluded a more systematic study of the potential energy surface.

Since the UV absorption experimentally observed are for the clusters that formed in aqueous solution, the effects of solvent on the cluster structure were considered by using the self-consistent isodensity polarizable continuum model.[40,41] We reoptimized the cluster structures in a dielectric continuum ($\epsilon = 78.5$) at the B3P86/SB level. Energetics were then reevaluated at B3P86/LB levels. Table 2 gives the geometries (Å, deg) for the monomer to the tetramer both in the gas phase and in a dielectric medium. Solvent does not affect the basic symmetry of the clusters, but it does result in generally longer bond lengths, as expected for a polar system. This effect decreases as the cluster size gets larger. For example, the Ag−Br bond length of the monomer in a dielectric medium increases by 0.0615 Å compared to the gas phase value, while it only increases by 0.0115 Å in the case of the tetramer. The larger clusters are affected even less.

The total energies (au) for monomer to nonamer in the gas phase and in a dielectric medium are shown in Table 3. The binding energy per molecule, E_B/n, is defined for neutral clusters as[48]

$$E_B/n = -E_n/n + E_1 = (-E_n + nE_1)/n \qquad (1)$$

where E_n is the energy of neutral clusters with n AgBr molecules. E_B/n is a measure of cluster stability.[49] A plot of E_B/n vs n is shown in Figure 3. The trends in binding energies shown in Figure 3 are similar to those for lithium and sodium neutral clusters.[48,50] The calculations using the LB basis set indicate that binding energies increase rapidly up to the trimer, and then level off.

UV Absorption Spectra of AgBr Clusters. We now address in a qualitative fashion the issue of the UV absorption of AgBr clusters, which show first a blue and then a red shift as the size increases. Although we cannot expect quantitative accuracy for the large clusters examined here, we can reasonably expect to reproduce the qualitative trends seen experimentally, and to understand the underlying bonding phenomena which result in the unusual blue shift. For each structure we have examined, the HOMO → LUMO excitation is symmetry-allowed and has a large oscillator strength. We shall employ three approaches: (1) correlation with the HOMO/LUMO gap, (2) direct calculation of the energy difference between the ground state singlet and the lowest energy triplet state, and (3) CIS calculations on the low-lying singlet states.

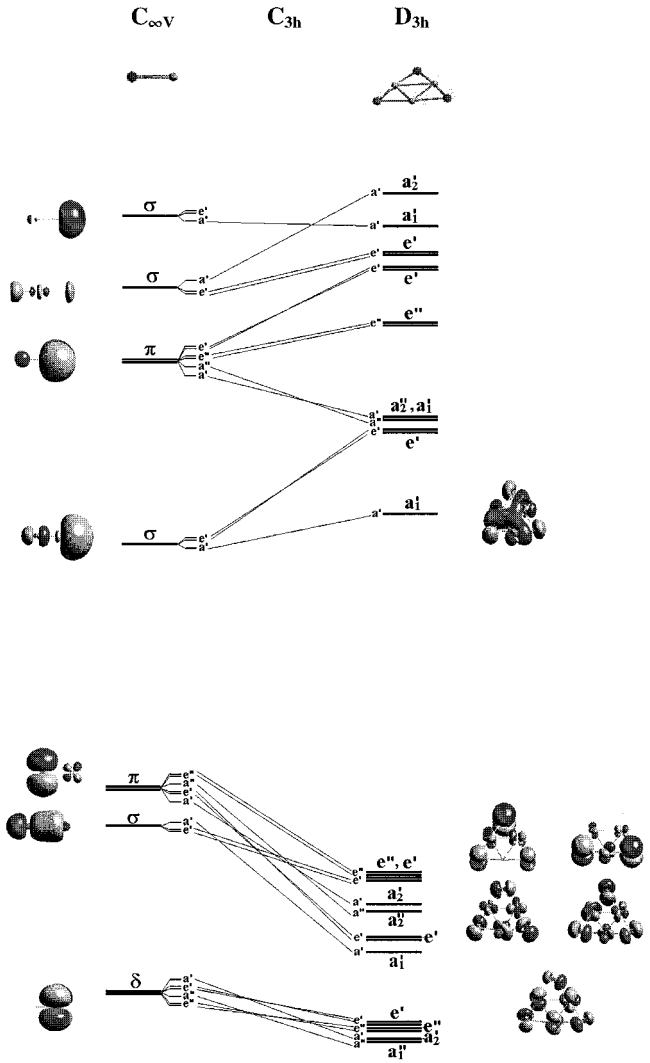

Figure 8. Molecular orbital energy level correlation diagram for trimerization.

Although the use of DFT one-electron energy differences to estimate excitation energies is a matter of debate,[51−53] Salzner et al.[54] recently presented results on 20 small- and medium-sized π-systems which show that HOMO−LUMO energy differences obtained with the B3LYP,[44,46] B3P86,[44,45] and B3PW91[55] functionals are in good agreement with vertical excitation energies from UV-absorption spectra. Figure 4 shows the DFT HOMO−LUMO gaps of the AgBr clusters at the B3P86/SB and B3P86/LB levels. It is clear that the energy gap increases as the AgBr clusters grow from the monomer to the trimer (blue shift) and then decreases as the AgBr clusters grow from the tetramer to the hexamer (red shift). This is exactly the trend observed experimentally. We have also calculated the HOMO−LUMO energy gaps in a dielectric medium. Solvent effects increase the HOMO−LUMO gap of monomer and dimer, but have little effect on clusters lager than the trimer.

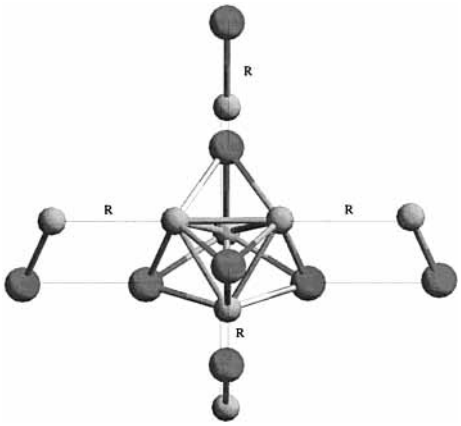

Figure 9. Formation of the tetramer from four monomers with overall D_{2d} symmetry.

The maximum blue shift is still located in the trimer in the dielectric medium. In all cases except the monomer, the HOMO−LUMO gaps overestimate the true energy differences.

The results are similar if we consider the vertical energy difference between the lowest triplet and singlet states ($\Delta E_{\text{singlet-triplet}}$). Calculation of the singlet−triplet gap has the advantage that both states can be calculated variationally; however, one would expect these values to underestimate the true UV absorption energies (Table 4). While these energies cannot be directly compared to the singlet−singlet energies observed in the UV spectra, they still should provide a qualitative indication of the general trends. The $\Delta E_{\text{singlet-triplet}}$ values in a dielectric medium are actually in reasonable accord with the experimental UV absorption energies and indicate a maximum blue shift at the trimer, with $\Delta E_{\text{singlet-triplet}} = 4.40$ eV (experimentally, the maximum blue shift occurs at 4.61 eV, but the cluster size of this species is not known).

We have also used the configuration interaction singles (CIS) method[40] to calculate the UV absorption energy of AgBr clusters at the CIS/SB and CIS/LB levels (the CIS calculations employed Hartree−Fock orbitals). The results for the first excitation energies from the monomer to the hexamer are listed in Table 4. The calculated spectra also show first a blue and then a red shift, with the maximum blue shift located at the tetramer. However, all of the CIS results predict much larger excitation energies than are observed experimentally. We conclude that

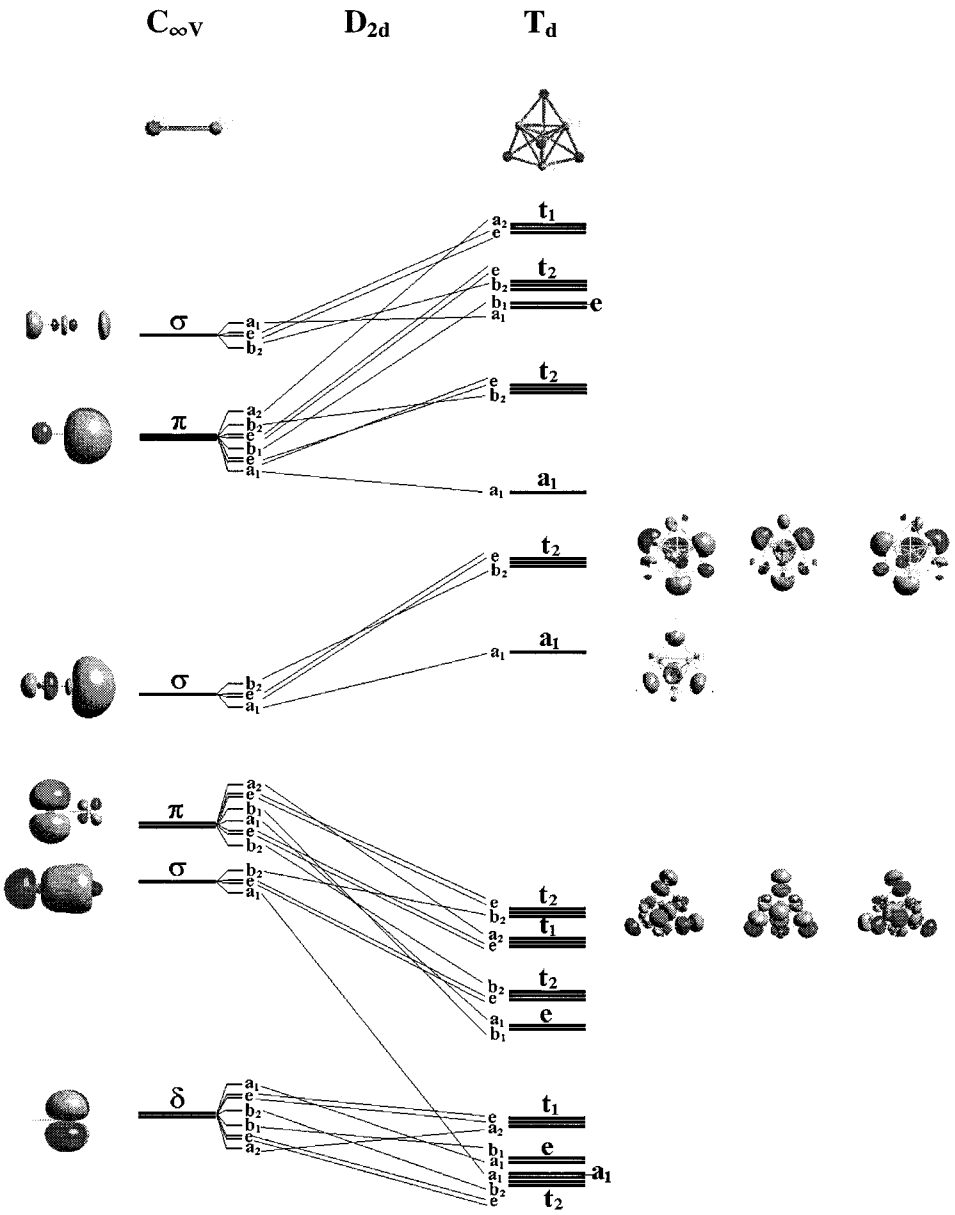

Figure 10. Molecular orbital energy level correlation diagram for tetramerization.

the qualitative trends observed experimentally are readily reproduced by even the simplest approaches (e.g., HOMO−LUMO gaps) but that quantitative calculations of the excitation energies will require much more sophisticated methodology.

Molecular Orbital Energy Level Correlation Studies of AgBr Dimerization, Trimerization, and Tetramerization. Now we turn to the second question we **p**roposed in the Introduction: What is the molecular origin of the first blue and then red shift? To answer this question, we must study how the molecular orbital energy levels change upon formation of a cluster from isolated monomers. Figure 5 illustrates how the dimer can be constructed from two monomers by varying only one geometrical parameter, and Figure 6 shows the resulting correlation diagram. Figures 7 and 8 (9 and 10) illustrate the same information for the trimer (tetramer).

For the dimerization, the monomer ($C_{\infty v}$) and the dimer (D_{2h}) share a common symmetry of C_{2h}. The HOMOs of the monomers are of π symmetry (essentially 4p orbitals on Br) which transform as $b_u + a_g + b_g + a_u$ in C_{2h} symmetry. The next lowest orbitals are of σ symmetry ($a_g + b_u$ in C_{2h}) and are dominantly bromine $4p_\sigma$ and silver $4d_{z^2}$ (the bromine 4s orbital is lower in energy that the silver 3d orbitals, and may to a first approximation be neglected). The next lowest orbitals are the Ag 4d orbitals of δ symmetry ($b_u + a_g + b_g + a_u$ in C_{2h}). The π type d orbitals are of lower energy and are not shown on the diagram. The LUMOs are predominately $5s/5p_\sigma$ silver atomic orbitals which transform as $a_g + b_g$ in C_{2h}. The second LUMOs are vacant 5p orbitals on Ag which transform as $b_u + a_g + b_g + a_u$ in C_{2h}. Thus, the first six HOMOs and the first six LUMOs transform as $2a_g + a_u + b_g + 2b_u$ in C_{2h}. It is the mixing of these orbitals which results in a stabilization of the occupied orbitals and a destabilization of the unoccupied orbitals. The net effect is an increase in the HOMO−LUMO gap, as illustrated in Figure 6. Note that only one of the occupied orbitals of the dimer (the a_g orbital arising from mixing of the two σ orbitals of the monomer) has significant Ag−Ag bonding character. This is a general trend also seen in the higher clusters: The short Ag−Ag interactions do not arise from strong Ag−Ag bonding, but rather from the fact that formation of silver clusters allows for the efficient overlap of bromine-occupied atomic orbitals with the unoccupied orbitals of several silver atoms. Indeed, the Ag−Ag Mulliken overlap[56,57] population at the B3P86/SB level is actually negative, and a natural bond order analysis[58,59] at the same level describes the dimer as having four Ag−Br bonds and no Ag−Ag bond.

The same process was used to obtain the correlation diagrams for trimerization and tetramerization. For trimerization (Figure 7), the common symmetry is C_{3h} (the symmetry of the trimer is D_{3h}), while for tetramerization (Figure 9), the common symmetry is D_{2d} (the symmetry of the tetramer is T_d). Upon proceeding from the dimer to the trimer, the number of Ag−Br interactions increases from four to six. This allows for increased orbital overlap between the HOMOs and LUMOs of the monomeric species and results in a larger HOMO−LUMO gap. One might expect the same phenomena to occur for the tetramer, where the number of Ag−Br interactions increases to 12, but the HOMO−LUMO gap actually decreases slightly in the gas phase, and remains about the same for the calculations done in a dielectric medium. Only the CIS calculations indicate that the actual point of maximum blue shift occurs at the tetramer level. Therefore, we cannot make a definitive statement as to where the maximum blue shift occurs, but it is certainly either at the trimer or tetramer level. As in the case of the dimer, Ag−Ag interactions are not the dominant feature in these clusters. Ag−Ag Mulliken overlap populations are again negative. As one proceeds to larger clusters, there are no longer enough bromine atoms to saturate all of the faces of the tetrahedra. This produces low-lying LUMOs localized on the empty faces of Ag_4 tetrahedra and lowers the HOMO−LUMO gap. Thus, the lowering of the HOMO−LUMO gap in this size regime is not associated with the classical QSE, but rather with the details of the orbital interactions between the formally filled bromine orbitals and empty orbitals of the silver polyhedra.

Summary

In summary, we have investigated the structures and UV absorption spectra of $(AgBr)_n$ clusters ($n = 1-9$) in both the gas phase and in a dielectric medium. The structures of clusters were determined at the B3P86/SB level with full geometry optimization and can generally be described as having Ag_4 tetrahedral moieties with bromine atoms capping the faces or bridging the edges of the silver tetrahedra. The calculated UV absorption peak of these structure, as modeled by a variety of simple approaches, indicate first a blue shift and then a red shift. Our computational results parallel the experimental trends and show that the point of maximum blue shift occurs at the trimer or tetramer region. The molecular origin of the blue/red shift associated with AgBr cluster growth can be readily explained by examining the orbital interactions which dominate the process and by the structure characterization of the clusters.

Acknowledgment. This work was supported in part by grants from the Welch Foundation to D.S.M. (Y-0743) and Z.A.S. (Y-0703), and from NSF to Z.A.S. (CHE-9509038).

Supporting Information Available: Cartesian coordinates and energies for all stationary points are available. This material is available free of charge via the Internet at http://pubs.acs.org.

References and Notes

(1) Brus, L. E. *J. Chem. Phys.* **1984**, *80*, 4403−4409.
(2) Bawendi, M. G.; Wilson, W. L.; Rothberg, L.; Carroll, P. J.; Jedju, T. M.; Steigerwald, M. L.; Brus, L. E. *Phys. Rev. Lett.* **1990**, *65*, 1623−1626.
(3) Norris, D. J.; Nirmal, M.; Murray, C. B.; Sacra, A.; Bawendi, M. G. *Z. Phys. D.* **1993**, *26*, 355−357.
(4) Archibong, E. F.; St.-Amant, A. *J. Chem. Phys.* **1998**, *109*, 962−972.
(5) Murray, C. B.; Nirmal, M.; Norris, B. J. Bawendi, M. G. *Z. Phys. D* **1993**, *26*, 231−233.
(6) *The Theory of the Photographic Process*; James, T. H., Ed.; Macmillan: New York, 1977.
(7) *Photographic Sensitivity*; Tadaaki, T., Ed.; Oxford University Press: New York, 1995.
(8) Ehrlich, S. H. *J. Imaging Sci. Technol.* **1994**, *38*, 201−216.
(9) Rossetti, R.; Hull, R.; Gibson, J. M.; Brus, L. E. *J. Chem. Phys.* **1985**, *83*, 1406−1410.
(10) Johannson, K. P.; McLendon, G. L.; Marchetti, A. P. *Chem. Phys. Lett.* **1991**, *179*, 321−324.
(11) Marchetti, A. P.; Johansson, K. P.; McLendon, G. L. *Phys. Rev. B* **1993**, *47*, 4268−4275.
(12) Matsumoto, Y.; Kawamura, Y.; Ohzeki, T.; Urabe, S. *Phys. Rev. B* **1992**, *46*, 1827−1830.
(13) Vogelsang, H.; Stolz, H.; von der Osten, W. *J. Lumin.* **1996**, *70*, 414−420.
(14) Chen, W.; Rehm, J. M.; Myers, C.; Freedhoff, M. I.; Marchetti, A.; McLendon, G. *Mol. Cryst. Liq. Cryst.* **1994**, *252*, 79−86.
(15) Brus, L. E. *J. Phys. Chem.* **1986**, *90*, 2555−2560.
(16) He, T.; Wang, P.; Zhang, X.; Liu, F. *Chin. J. Chem. Phys.* **1995**, *8*, 23−27.
(17) Alivisatos, A. P. *Science* **1996**, *271*, 933−937.
(18) *Optical Properties of Semiconductor Quantum Dots*; Woggon, U., Ed.; Springer-Verlag: New York, 1997.
(19) Zhang, H.; Mostafavi, M. *J Phys. Chem. B* **1997**, *101*, 8443−8448.

(20) (a) Schelly, Z. A.; Correa, N. M.; Zhang, H. *Proc. 215th ACS National Meeting, Div. Colloid Surf. Chem.* (*Dallas, TX, March 29−April 2, 1998*) **1998**, 116. (b) Correa, N. M.; Zhang, H.; Schelly, Z. A. *J. Am. Chem. Soc.*, in press.
(21) Kunz, A. B. *Phys. Rev. B.* **1982**, *26*, 2070−2075.
(22) Onwuagba, B. N. *Solid State Commun.* **1996**, *97*, 267−271.
(23) Victora, R. H. *Phys. Rev. B.* **1997**, *56*, 4417−4421.
(24) Nunes, G. S.; Allen, P. B.; Martins, J. L. *Solid State Commun.* **1998**, *105*, 377−380.
(25) Ozin, G. A.; Huber, H.; Mcintosh, D.; Mitchell, S.; Norman, J. C., Jr.; Noodleman, L. *J. Am. Chem. Soc.* **1979**, *101*, 3504−3511.
(26) Walch, S. P.; Bauschlicher, C. W., Jr.; Langhoff, S. R. *J. Chem. Phys.* **1986**, *85*, 5900−5906.
(27) Walch, S. P. *J. Chem. Phys.* **1987**, *87*, 6776−6778.
(28) Liao, D. W.; Balasubramanian, K. *J. Chem. Phys.* **1992**, *97*, 2548−2552.
(29) Bonacic-Koutecky, V.; Cespiva, L.; Fantucci, P.; Koutecky, J. *J. Chem. Phys.* **1993**, *98*, 7981−7994.
(30) Santamaria, R.; Kaplan, I. G.; Novano, O. *Chem. Phys. Lett*. **1994**, *218*, 395−400.
(31) He, T.; Cui, W.; Liu, F. *Chin. J. Chem. Phys.* **1996**, *9*, 330−333.
(32) He, T.; Liu, F. *Imaging Sci. J.* **1997**, *45*, 57−60.
(33) Andzelmt, J.; Klobukowski, M.; Radzio-Andzelm, E. *J. Comput. Chem.* **1984**, *5*, 146−161.
(34) Muller, H. *Theor. Chim. Acta* **1971**, *21*, 110−114.
(35) Schuster, P.; Mikosch, H.; Bauer, G. *J. Chem. Phys*. **1998**, *109*, 1833−1844.
(36) Rabilloud, F.; Spiegelmann, F.; Heully, J. L. *J. Chem. Phys.* **1999**, *111*, 8925−8933.
(37) *Gaussian 94* (Revision D.4); Frisch, M. J.; Trucks, G. W.; Schlegel, H. B.; Gill, P. M. W.; Johnson, B. G.; Robb, M. A.; Cheeseman, J. R.; Keith, T. A.; Petersson, G. A.; Montgomery, J. A.; Raghavachari, K.; Al-Laham, M. A.; Zakrzewski, V. G.; Ortiz, J. V.; Foresmans, J. B.; Cioslowski, J.; Stefanov, B. B.; Nanayakkara, A.; Challacombe, M.; Peng, C. Y.; Ayala, P. Y.; Chen, W.; Wong, M. W.; Andres, J. L.; Replogle, E. S.; Gomperts, R.; Martin, R. L.; Fox, D. J.; Binkley, J. S.; Defrees, D. J.; Baker, J.; Stewart, J. P.; Head-Gordon, M.; Gonzalez, C.; Pople, J. A. Gaussian, Inc.: Pittsburgh, PA, 1995.
(38) Schaefer, A.; Huber, C.; Ahlrichs, A. *J. Chem. Phys.* **1994**, *100*, 5829−5835.
(39) The silver basis sets was obtained from the Extensible Computational Chemistry Environment Basis Set Database, Version 1.0, as developed and distributed by the Molecular Science Computing Facility, Environmental and Molecular Sciences Laboratory, which is part of the Pacific Northwest Laboratory, P.O. Box 999, Richland, WA 99352, and funded by the, U.S. Department of Energy. The Pacific Northwest Laboratory is a multiprogram laboratory operated by Battelle Memorial Institute for the, U.S. Department of Energy under contract DE-AC06-76RLO 1830. Contact David Feller, Karen Schuchardt, or Don Jones for further information.
(40) *Exploring Chemistry with Electronic Structure Methods*; Foresman, J. B., Frisch, M. J., Eds.; Gaussian, Inc.: Pittsburgh, PA, 1996.
(41) Wiberg, K. B.; Keith, T. A.; Frisch, M. J.; Murcko, M. *J. Phys. Chem.* **1995**, *99*, 9072−9079.
(42) Berkowitz, J.; Batson, C. H.; Goodman, G. L. *J. Chem. Phys.* **1980** *72*, 5829−5837.
(43) Nair, K. P. R.; Hoeft, J. *Phys. Rev. A* **1987**, *35*, 668−672.
(44) Becke, A. D. *J. Chem. Phys.* **1993**, *98*, 5648−5657.
(45) Perdew, J. P. *Phys. Rev. B.* **1986**, *33*, 8822−8824.
(46) Lee, C.; Yang, W.; Parr, R. G. *Phys. Rev. B* **1988**, *37*, 785−789.
(47) Becke, A. D. *Phys. Rev. A.* **1988**, *38*, 3098−3100.
(48) Boustani, I.; Pewestorf, W.; Fantucci, P.; Bonacic-Koutecky, V.; Koutecky, J. *Phys. Rev. B* **1987**, *35*, 9437−9450.
(49) Boustani, I.; Koutecky, J. *J. Chem. Phys.* **1988**, *88*, 5657−5662.
(50) Bonacic-Koutecky, V.; Fantucci, P.; Koutecky, J. *Phys. Rev. B* **1988**, *37*, 4369−4374.
(51) Oliveira, L. N.; Gross, E. K. U.; Kohn, W. *Phys. Rev. A* **1988**, *37*, 2821−2833.
(52) Levy, M. *Phys. Rev. A* **1995**, *52*, R4313−R4315.
(53) Nesbet, R. K. *J. Phys. Chem.* **1996**, *100*, 6104−6106.
(54) Salzner, U.; Lagowski, J. B.; Pickup, W.; Poirier, R. A. *J. Comput. Chem.* **1997**, *18*, 1943−1953.
(55) Perdew, J. P.; Wang, Y. *Phys. Rev. B* **1992**, *45*, 13244−13249.
(56) Mulliken, R. S. *J. Chem. Phys.* **1955**, *23*, 1833−1840.
(57) Holger, W.; Werner, K. *J. Am. Chem. Soc.* **1979**, *101*, 2804−2814.
(58) Foster, J. P.; Weinhold, F. *J. Am. Chem. Soc.* **1980**, *102*, 7211−7218.
(59) Reed, A. E.; Curtiss, L. A.; Weinhold, F. *Chem. Rev.* **1988**, *88*, 899−926.
(60) Hay, P. J.; Wadt, W. R. *J. Chem. Phys.* **1985**, *82*, 299−310.